Signaling compartment at the ciliary tip is formed and maintained by intraflagellar transport and functions as sensitive salt detector

Servaas N. van der Burght[1], Suzanne Rademakers[1], Jacque-Lynne Johnson[2,3], Chunmei Li[2,3], Michel R. Leroux[2,3], Gert Jansen[1]

[1]Dept. of Cell Biology, Erasmus MC, Rotterdam, The Netherlands
[2]Dept. of Molecular Biology and Biochemistry, Simon Fraser University, Burnaby, B.C., Canada
[3]Centre for Cell Biology, Development, and Disease, Simon Fraser University, Burnaby, B.C., Canada

ABSTRACT

Primary cilia are ubiquitous antenna-like organelles that mediate cellular signaling and represent hotspots for human diseases termed ciliopathies. How signaling subcompartments are established within the microtubule-based organelle, and for example support Hedgehog or cGMP signal transduction pathways, remains a central question. Here we show that a *C. elegans* salt-sensing receptor type guanylate cyclase, GCY-22, accumulates at a very high concentration within the distal region of the cilium. This receptor uses DAF-25 (Ankmy2 in mammals) to cross the transition zone (TZ) membrane diffusion barrier in the proximal-most region of the ciliary axoneme. Targeting of GCY-22 to the ciliary tip is dynamic, requiring the cargo-mobilizing intraflagellar transport (IFT) system. Disruption of transit across the TZ barrier or IFT trafficking causes GCY-22 protein mislocalization and defects in the formation, maintenance, and function of the ciliary tip compartment required for chemotaxis to low NaCl concentrations. Together, our findings reveal how a previously undescribed cilium tip cGMP signaling compartment is established and contributes to the physiological function of a primary cilium.

INTRODUCTION

The primary cilium is a specialized signaling organelle used by metazoan cells to receive and propagate cues from their environment. The receptor and signaling proteins that enable cilia to perform their functions must reach and remain at their correct sub-ciliary position and concentration. Defects in the localization and/or functions of ciliary signaling components are associated with a wide range of diseases, including multi-syndromic Bardet-Biedl (BBS), Meckel, and Joubert syndromes (Reiter & Leroux 2017). However, our understanding of the regulation of protein localization in cilia from different cell types, and their relevance to creating functional signaling domains, is limited.

Cilia use at least two major mechanisms, a trafficking system and a diffusion barrier, that function together to dynamically regulate the trafficking of proteins into, out of, and within cilia. The main trafficking machinery used by cilia is called intraflagellar transport (IFT). This system facilitates the bidirectional transport of ciliary cargo, including signaling proteins, from the base/foundation of the organelle (basal body) to the tip of the ciliary axoneme (Lechtreck 2015). Anterograde movement of IFT trains to the tip is propelled by kinesins, and a cytoplasmic dynein enables retrograde transport back to the base. Two IFT modules, termed subcomplexes A and B, as well as another module containing BBS proteins (BBSome) that is thought to bridge the two subcomplexes, play essential roles in cargo transport (Liu & Lechtreck 2018; Klink et al. 2017). The best-known IFT cargos are structural components of the axoneme, including tubulin (Hao et al. 2011), but signaling proteins, such as the *C. elegans* TRPV channel subunits OSM-9 and OCR-2, have also been identified as IFT cargos (Qin et al. 2005). Additionally, several mammalian ciliary signaling proteins, namely the GPCR SSTR3 and the Hedgehog (Hh) signaling component SMO, are known to traverse the cilium by both IFT and diffusion (Ye et al. 2013).

To help confine proteins to cilia, a diffusion barrier for both membrane and soluble proteins is present at the ciliary base (Ye et al. 2018; Prevo et al. 2015; Ludington et al. 2013). For membrane-associated proteins, this functionality is ascribed to the transition zone (TZ), a ciliary subdomain immediately distal to the basal body. How the TZ acts with the IFT system to influence the movement of proteins across this region and regulate the composition of the sensory organelle is not well understood.

Signaling proteins can have different sub-ciliary localizations, including the proximal or distal segments, or ciliary tip. For example, in the cilia of *C. elegans* the cyclic nucleotide gated channel TAX-2 localizes to the proximal region adjoining the transition zone (Wojtyniak et al. 2013). Other proteins, like the TRPV channel subunits OSM-9 and OCR-2 (Qin et al. 2005) and several GPCRs (Kim et al. 2009; McGrath et al. 2011; Wojtyniak et al. 2013), localize along the length of the cilium. In mammals, the kinesin-like protein KIF7 and the Hh signaling components SUFU and GLI2 localize at the cilium tip (Liem et al. 2009; Endoh-Yamagami et al. 2009; He et al. 2014). Mislocalization of ciliary proteins can have serious repercussions for signaling and development. For example, mislocalization of PDE6 and GRK1 in mammalian photoreceptor cells can lead to retinitis pigmentosa (Zhang et al. 2014) and mice mutant for the BBSome subunit BBS2 exhibit neurosensory defects and retinopathy, presumably caused by mislocalized rhodopsin (Nishimura et al. 2004). Another compartment, present in the proximal region of the cilium, uses Inversin (NPHP2) and other proteins to modulate Wnt signaling (Lienkamp et al. 2012). Despite their importance, the mechanisms that govern how signaling components concentrate along specific regions of cilia, rather than their entire length, remain unknown.

To explore these important aspects of cellular signaling, we use the cilium-dependent response of *C. elegans* to NaCl as a model to understand the underlying molecular mechanisms of signaling domain formation, maintenance and function. In *C. elegans*, attraction to NaCl is mediated by the two

bilateral ASE (Amphid Single ciliated ending E) head neurons, which express multiple receptor-type guanylate cyclases, including *gcy-14* (ASEL) and *gcy-22* (ASER) (Ortiz et al. 2009; Ortiz et al. 2006; Etchberger et al. 2007). Behavioral and Ca^{2+} imaging experiments indicate that GCY-22 is required for the response to Cl^-, and GCY-14 for responding to Na^+ (Ortiz et al. 2006; Ortiz et al. 2009; Smith et al. 2013).

By endogenously tagging GCY-22 with GFP, we discovered that the guanylate cyclase is present at a high concentration in a cilium tip compartment. We demonstrate that this GCY-22 localization depends on the IFT machinery, including the BBS complex. We further show that DAF-25, the ortholog of the poorly-studied mammalian protein Ankmy2, is required for GCY-22 entry into the cilium, and hence localization to the tip compartment. Using structure-function studies, we identified GCY-22 protein domains required for cilium entry and localization at the tip. Disrupting the localization of the receptor at the tip compartment hinders the ability of *C. elegans* to detect low concentrations of NaCl. On the whole, our findings provide mechanistic insights into the formation and maintenance of a novel ciliary subdomain essential for cGMP-mediated cellular signaling.

RESULTS

GCY-22::GFP is highly concentrated at the ASER ciliary tip and periciliary membrane compartment

We used CRISPR/Cas9 to endogenously tag the *gcy-22* gene with *GFP* and determine the sub-cellular localization of this receptor-type guanylate cyclase in the ASER neuron. Confocal microscopy and co-labeling with markers for the ER (*tram-1*) and trans Golgi (*apt-9*) revealed that GCY-22::GFP is present within the ER and trans-Golgi compartment in the cell body (Fig.1A, Sup. Fig. 1.). In the dendrite, time-lapse imaging revealed anterograde and retrograde transport of GCY-22::GFP (Sup. Fig. 2.), reminiscent of kinesin and dynein-mediated transport of vesicles (Mondal et al. 2011). At the end of the dendrite, GCY-22::GFP is abundant at the periciliary membrane compartment (PCMC), a vestibule of the cilium (Fig. 1A).

The most striking localization of GCY-22::GFP in ASER is in the cilium, where GCY-22::GFP is highly enriched at the ciliary tip (Fig. 1A), but not along the length of the axoneme where most other receptors analyzed thus far are located (L'Etoile & Bargmann 2000; Birnby et al. 2000; Takeishi et al. 2016). We expressed GCY-22::GFP under an ASI specific promoter to determine if the tip localization is cell type dependent. GCY-22::GFP localized to the ciliary tip in low amounts (Fig 1B), suggesting a mechanism that is possibly not cell specific.

The strong fluorescent signal at the tip of ASER cilia suggested the presence of a large number of GCY-22::GFP molecules. Using a purified GFP sample as reference, we estimated the concentration of GCY-22::GFP in the cilium tip to be 2.77 mM, reflecting a density of approximately 110,575 (±31,998) molecules/μm^2 (Fig. 1C). The only example of a receptor with a comparable density we are aware of is rhodopsin in the disks of the rod outer segment of the mammalian photoreceptor. In these cilia, rhodopsin is present at densities of up to 48,300 molecules/μm^2 (Fotiadis et al. 2003; Niu & Mitchell 2005), which allows the photoreceptors to respond to single photons (Rieke & Baylor 1998). This suggests that the ciliary tip compartment of the ASE neurons could function as a highly sensitive detector of NaCl.

GCY-22::GFP exists in stable pools at the periciliary membrane and ciliary tip

To determine how the pools of GCY-22::GFP present at the ciliary tip and PCMC are replenished, we used a Fluorescent Recovery after Photobleaching (FRAP) assay. Recovery of GCY-22::GFP after photobleaching of the entire ciliary tip was modest (7% after 25 min) indicating little or slow transport

towards the cilium tip (Fig. 2A). Recovery after photobleaching of the entire PCMC (28% after 25 min) was faster than at the ciliary tip, potentially reflecting continuous transport of GCY-22::GFP from the cell body to the dendritic terminus (Fig. 2B).

To determine the motility of GCY-22::GFP *within* the ciliary tip and the PCMC, we photobleached half of these compartments. Within the ciliary tip, fluorescence was maximally recovered in 3-4 minutes ($t_{1/2}$ = 54.89 sec.) and showed complete redistribution of GCY-22::GFP within the tip (Fig. 2C), demonstrating lateral diffusion within the tip compartment. Partial photobleaching of GCY-22::GFP at the PCMC resulted in recovery of fluorescence in 60 seconds ($t_{1/2}$=11.43 sec.) (Fig. 2D), significantly faster than in the ciliary tip. Together, these data show that GCY-22 is present in the PCMC and cilium tip of ASER in large and stable pools, suggesting that there is limited, or slow, exchange between these compartments. The motility of GCY-22::GFP within the ciliary tip appears more restricted than at the PCMC.

Ciliary tip compartment of GCY-22::GFP depends on active IFT

Because the proximal region of the axoneme (middle segment) and part of the distal segment of the cilium seemed void of GCY-22::GFP, we hypothesized that it might be actively transported from the PCMC to the ciliary tip by the IFT machinery. In *C. elegans*, the IFT machinery relies on two kinesins (kinesin-II and OSM-3) for anterograde movement along the middle segment and on OSM-3 alone for transport within the distal segment of the axoneme.

Using time-lapse microscopy and kymograph analysis, we identified GCY-22::GFP particles moving between the PCMC and ciliary tip (Fig. 3A). To determine if the GCY-22::GFP particles are transported by the IFT machinery, we performed two-color imaging of GCY-22::GFP and an mCherry-tagged version of the OSM-3 anterograde IFT kinesin, the ortholog of mammalian KIF17 (Fig. 3B). These experiments showed GCY-22::GFP anterograde tracks overlapping with those of OSM-3::mCherry. We observed on average 37.8 (± 8.4) anterograde OSM-3::mCherry tracks per minute but only 6.14 (± 3.61) anterograde and 6.71 (± 3.71) retrograde GCY-22::GFP tracks per minute, suggesting that only a subset of IFT particles is used to transport GCY-22::GFP as cargo (Table 1).

In contrast to IFT particles that often move along the full length of the cilium (average track length 2.75 ± 0.54 µm), anterograde GCY-22::GFP particles display shorter tracks, spanning half of the cilium or shorter (average track length 1.0 ± 0.4 µm, $P<0.001$, Fig. 3C). Retrograde transport of GCY-22::GFP was also observed, in short tracks and occasionally in tracks spanning the entire axoneme, together averaging 1.3 ± 0.8 µm in length (Fig. 3C). These are significantly shorter than retrograde tracks from the core IFT protein, OSM-3 (average track length 2.12 ± 0.59 µm, $P<0.001$). In many animals, particles appeared to pause halfway along the cilium, as indicated by a stationary fluorescence signal in the kymograph that possibly reflects the end of the middle segment (Fig. 3A). Interestingly, the GCY-22::GFP tracks frequently changed from a retrograde to an anterograde direction, docking with an anterograde OSM-3::mCherry track and moving towards the tip compartment (Fig. 3B). This is notable, as this behavior is not observed for core IFT proteins. These data suggest that GCY-22::GFP particles that move from the tip into the cilium are targeted back to the tip by the anterograde IFT machinery, keeping the GCY-22::GFP clear of the ciliary axoneme and concentrated at the tip.

To study the contribution of IFT to cilium tip localization, we visualized the localization of GCY-22::GFP in different IFT mutant backgrounds. Disruption of the anterograde kinesin-II subunit KAP-1, which plays a role in entry of IFT particles into the cilium (Oswald et al. 2018), did not affect GCY-22::GFP levels in the cilium or its localization (Fig. 3D,E). In this *kap-1(ok676)* mutant, the middle and distal segments are present, as the remaining OSM-3-kinesin can transport cargo to the cilium tip and

build the entire axoneme. In contrast, the *osm-3(p802)* mutant, which lacks functional OSM-3 and therefore a distal segment, has no GCY-22::GFP at the tip of the middle segment and shows increased levels of GCY-22::GFP in the PCMC and along the remaining axoneme (Fig. 3D,E). Loss of BBS-8, a subunit of the BBSome complex believed to act as an adaptor between the IFT machinery and some cargo proteins (Nakayama & Katoh 2018), reduced the overall level of GCY-22::GFP in the cilium, including at the tip, while increasing the amount of the guanylate cyclase along the length of the cilium (Fig. 3D,E). The changes in GCY-22::GFP localization in *osm-3(p802)* and *bbs-8(nx77)* mutants correlate with a significant decrease in GCY-22::GFP tracks (Table 1), suggesting that loss of OSM-3 or BBS-8 alters the transport dynamics of cargo proteins such as GCY-22::GFP. Taken together, our results show that the kinesin-II subunit KAP-1 is not required for import of GCY-22::GFP into the cilium, and that both OSM-3 mediated IFT and the BBSome are important for its transport in the cilium and enrichment at the tip.

We reasoned that if IFT is responsible for the ciliary tip localization of GCY-22::GFP, interrupting the transport machinery should alter or abolish GCY-22::GFP tip localization. To test this, we used NaN_3 to stop ATP production and as a result stop IFT over time. OSM-3::mCherry particles slowed down and became less frequent after 10 minutes of NaN_3 treatment (Fig. 4A). IFT capacity, which we define as the number of IFT tracks multiplied by their speed, reached 0 after 30-50 min of NaN_3 treatment (Fig. 4B). During treatment, the length of the cilium steadily shortened, while the GCY-22::GFP compartment started to extend into the cilium after 10 minutes in some animals and completely collapsed after 20-30 minutes of NaN_3 treatment (Fig. 4A,B). Importantly, the loss of cilium tip localization after 30 minutes of NaN_3 treatment was reversible, with complete recovery of the cilium tip within 16 minutes (Fig. 4C). These experiments suggest that a certain minimal IFT capacity is required to maintain GCY-22::GFP localization at the cilium tip, although we cannot exclude that the effect of NaN_3 treatment might be mediated by an IFT-independent mechanism. Additionally, GCY-22::GFP relocalization into the cilium during NaN_3 treatment occurs abruptly whereas cilium length changes gradually, suggesting that these are independent processes.

Taken together, these experiments show that IFT plays an important role in actively maintaining the high GCY-22 concentration at the ciliary tip.

GCY-22 trafficking and cilium import is regulated by the transition zone and requires DAF-25

The accumulation of a large pool of membrane-associated GCY-22::GFP at the PCMC suggests that the guanylate cyclase is prevented from readily diffusing into the cilium. The transition zone, just distal to the PCMC, is thought to form a membrane diffusion barrier that creates a ciliary membrane compartment distinct from that of the cell body and PCMC (Garcia et al. 2018). We therefore tested the hypothesis that the TZ restricts ciliary entry of GCY-22::GFP.

We first tested whether ablation of the TZ allows for GCY-22::GFP entry into the cilium. Surprisingly, loss of MKS-5 (a mammalian RPGRIP1/RPGRIP1L ortholog), which removes all known proteins from the TZ as well as the characteristic Y-link structures (Williams et al. 2011; Brear et al. 2014), has a relatively subtle effect on GCY-22::GFP localization. GCY-22::GFP mislocalized at the TZ and base of the ciliary axoneme and the amount localizing at the cilium tip was reduced (Fig. 3D,E). We did not see increased entry of GCY-22::GFP molecules, suggesting that the TZ is not the only mechanism preventing GCY-22::GFP entry into the cilium.

The Ankmy2 protein DAF-25 was previously identified as required for ciliary localization of guanylate cyclases (Jensen et al. 2010; Fujiwara et al. 2010; Brear et al. 2014), cyclic nucleotide gated channels and GPCRs (Wojtyniak et al. 2013; Brear et al. 2014), but not for IFT (Jensen et al. 2010). To study if DAF-25 contributes to the trafficking of GCY-22::GFP into the cilium, we introduced GCY-22::GFP

into *daf-25(m362)* animals. Remarkably, GCY-22::GFP did not enter the cilium and we observed no GCY-22::GFP IFT tracks and no ciliary tip localization in these mutant animals (Fig. 3D-E, Table 1.) Interestingly, *daf-25(m362)* animals showed lower levels of GCY-22::GFP at the PCMC and only very few moving vesicles and diffuse fluorescence in the dendrite (Fig. 3E, Sup. Fig. 2.). In the cell body, GCY-22::GFP localization was more dispersed than in WT animals, and did not overlap with the trans-Golgi marker APT-9::mCherry (Sup. Fig. 1, 3). These results suggest that DAF-25 plays a role in early trafficking, as well as facilitating the entry of GCY-22::GFP into the cilium.

To test if DAF-25 functions together with the TZ to traffic GCY-22::GFP into the cilium, we generated a *daf-25(m362); mks-5(tm3100)* mutant strain. In this double mutant, we observed low levels of GCY-22::GFP in the cilium but no cilium tip compartment was formed (Fig. 3D,E). Very few IFT tracks of GCY-22::GFP were visible, potentially explaining the lack of cilium tip localization (Table 1). Because OSM-3 mediated IFT is not affected in *daf-25(m362); mks-5(tm3100)* animals (Table S1), MKS-5 and DAF-25 may be required to link GCY-22::GFP to the IFT machinery, allowing for the formation of the cilium tip compartment.

Together, our data show that DAF-25 is required for transport of GCY-22::GFP to the cilium and facilitates import across the TZ, and together with MKS-5 is involved in loading GCY-22::GFP as IFT cargo.

GCY-22::GFP localization requires its dimerization and RD3-associated domains

To identify protein domains required for the correct trafficking of GCY-22::GFP to the cilium tip, we generated a series of deletion constructs. Several domains can be recognized in GCY-22, including an extracellular receptor domain which possibly provides specificity for Cl^- ions (Ortiz et al. 2009; Smith et al. 2013). However, which protein domains are involved in its localization remains unexplored. We deleted the extra-cellular receptor domain and signaling peptide, or, the intra-cellular guanylate cyclase domain, dimerization domain, or c-terminal tail. Of these GFP-tagged deletion constructs, only the dimerization domain proved to be required for cilium entry (Fig. 5).

In addition, GCY-22 contains a protein domain at its C-terminus which shows homology to the RD3-binding domain identified in the mammalian guanylate cyclase GUCY2D/GC1 (Azadi et al. 2010). In mammals, the protein RD3 (Retinal Degeneration 3) is required for the localization of guanylate cyclase GUCY2D to the photoreceptor outer segment and has been implicated in the eye-specific ciliopathy Leber Congenital Amaurosis (LCA) (Zulliger et al. 2015). We made a deletion construct to determine if this domain is required for the trafficking of GCY-22 to the tip of the cilium. In a *gcy-22(lf)* background, GCY-22(ΔRD3)::GFP was localized at the PCMC but did not enter the cilium (Fig. 5). To confirm that the RD3 domain is required for cilium import, we replaced the 8 amino acids (W1042-I1049) of this domain with alanine residues in the GFP-tagged, endogenous *gcy-22* locus using CRISPR/Cas9 (GCY-22(RD3-Ala)::GFP). Mutation of the RD3 domain completely abolished ciliary entry (Fig. 3D,E). We also observed changes in the localization in the cell body and the dendrite, reflecting a potential defect in the routing of GCY-22(RD3-Ala)::GFP (Sup. Fig. 3).

Next, we tested if the RD3 domain is sufficient for cilium entry by generating two constructs containing the RD3 domain fused to the transmembrane (TM) domain and GFP, in two orientations: TM-RD3-GFP and TM-GFP-RD3. These proteins showed diffuse localization in the cell body, some vesicular transport in the dendrite, and localization at the PCMC. We observed a very weak signal in the cilium but could not detect transport by IFT (Fig. 5, Sup Fig. 4). These results suggest that the RD3 domain is not sufficient for correct routing and import in the cilium.

In *C. elegans*, the RD3 orthologue is RDL-1. Disrupting RDL-1 function affects trafficking of GCYs from the Golgi to the cilium, resulting in reduced levels of protein in the cilium and PCMC (Martínez-Velázquez & Ringstad 2018). We observed reduced GCY-22::GFP levels in the PCMC but WT levels in the cilium tip (Fig. 3D,E). In addition, the localization of GCY-22::GFP in the cell body and dendrite was affected in *rdl-1* animals (Sup. Fig 1, 3), in agreement with a function of RDL-1 in an early trafficking pathway for GCYs.

In contrast to GCY-22::GFP, the guanylate cyclase DAF-11 localizes along the entire length of the cilium in ASI, ASJ, ASK neurons (Jensen et al. 2010; Birnby et al. 2000). We replaced the TM domain of GCY-22 with that of DAF-11 to see if the TM domain influences the specific localization of GCY-22. The TM of DAF-11 had no apparent effect on cilium tip localization (Fig. 5).

Together, our data show that the dimerization domain and the RD3 domain are required for entry of GCY-22 into the cilium. In addition, our data suggest that the RD3 domain is important, but not sufficient for cilium entry. Deletion of any of the other GCY-22 protein domains by themselves did not affect cilium tip localization, suggesting that this localization is regulated by the combined action of several domains.

GCY-22::GFP cilium tip compartment is required for high NaCl sensitivity

The ASE neurons express several receptor-type guanylate cyclases, of which GCY-22 and GCY-14 appear to be most important for the detection of NaCl (Ortiz et al. 2009; Ortiz et al. 2006; Smith et al. 2013). We tested *gcy-22(tm2364)* and *gcy-14(pe1102)* loss-of-function mutants and a *gcy-14; gcy-22* double mutant in a NaCl chemotaxis assay. In this quadrant assay, animals are tested for their preference for a particular NaCl concentration (contained within two quadrants) versus no NaCl (in the other two quadrants) (Wicks et al. 2000). *gcy-22::GFP* animals showed a wild type NaCl chemotaxis response. The *gcy-22(tm2364)* mutation significantly affected the chemotaxis response to NaCl, whereas the *gcy-14* mutant showed no defect (Fig. 6A). The double mutant did not have a significantly stronger defect than the *gcy-22* single mutant, suggesting that GCY-22 is the most important of the two guanylate cyclases in our NaCl chemotaxis assay (Fig. 6A).

To determine if the localization of GCY-22 at the cilium tip is important for *C. elegans'* sensitivity to NaCl, we first tested the IFT mutants for their chemotaxis response. *kap-1(ok676)* animals showed a wild type response to NaCl (Fig. 6B), consistent with the normal localization of GCY-22::GFP at the ciliary tip. *bbs-8(nx77)* animals showed reduced chemotaxis to 1 mM NaCl ($P<0.01$; Fig. 6B), which correlates with the reduced levels of GCY-22::GFP at the ciliary tip. *osm-3(p802)* animals, which have short cilia where GCY-22::GFP localizes along its entire length, showed the strongest chemotaxis defect at all NaCl concentrations tested ($P<0.01$; Fig. 6B).

Next, we tested *daf-25(m362)* animals, which have no ciliary GCY-22::GFP, for their chemotaxis response. These animals showed a very strong chemotaxis defect, with only a modest response to the highest (100 mM) NaCl concentration (Fig. 6C). This suggests that *daf-25* is required for the trafficking and ciliary import of proteins essential for chemotaxis to NaCl, in accordance with the mislocalization of guanylate cyclases and CNGs in this mutant (Fujiwara et al. 2010; Wojtyniak et al. 2013; Jensen et al. 2010). Surprisingly, *mks-5(tm3100); daf-25(m362)* double mutants showed a partially restored response to 10 mM NaCl and a wild-type response to 100 mM (Fig. 6C). These responses roughly correlate with the levels of GCY-22::GFP in the cilium in these mutants, and suggest that the levels of GCY-22::GFP that entered the cilium in the double mutant are sufficient for detecting high NaCl concentrations.

Together, our findings provide evidence that a high level of GCY-22 at the ciliary tip is required for highly sensitive NaCl detection. However, the possibility remains that in the mutants analyzed, other proteins that play a role in NaCl sensory transduction are affected, leading to the observed chemotaxis defects.

To specifically test the contribution of GCY-22::GFP ciliary tip localization to NaCl sensation, we tested the RD3-Ala mutant animals for their chemotaxis response. These animals showed a mild chemotaxis defect at 1 mM NaCl (P=0.023), but wild-type responses to 10 and 100 mM NaCl (Fig. 6D). The WT responses of the RD3-ala mutant animals at higher concentrations suggest that a small amount of GCY-22 could still be present in the cilium, or that the localization at the PCMC is sufficient for at least some of the animals' response to NaCl. Additionally, a chemotaxis defect in these animals could be masked by functional redundancy between the many guanylate cyclases. To test this latter possibility, we made a *gcy-14(pe1102); gcy-22(RD3-Ala)* double mutant and observed a stronger chemotaxis defect at 10 mM NaCl (P=0.020) than the *gcy-22(RD3-ala)* single mutant (Fig. 6D). Interestingly, *gcy-14(pe1102); gcy-22(RD3-Ala)* animals showed stronger chemotaxis to 100 mM NaCl than *gcy-14(pe1102); gcy-22(tm2364)* animals (P=0.004), indicating that the GCY-22 protein in which the RD3 domain has been replaced by Alanine residues is partially functional in detecting NaCl.

Together these experiments show that GCY-22 is required at the cilium tip for the detection, and efficient chemotaxis to low concentrations of NaCl.

DISCUSSION

Several signaling proteins localize to specific ciliary subdomains, whereas others localize along the length of the cilium, suggesting that these specific localizations are functionally important. Although ciliary signaling is important in physiology and development, our understanding of how the localization of signaling proteins within the cilium is regulated remains limited. Here, we identified mechanisms involved in the localization of the putative Cl^- receptor GCY-22 to a unique ciliary tip domain in the ASER neuron of *C. elegans*, and provide evidence that this specific localization is required for its function as a highly sensitive NaCl sensor.

Cilium entry

To function, GCY-22, trafficked to the periciliary membrane compartment, must cross the transition zone (TZ) before reaching the cilium. The TZ is a highly organized structure that acts as a diffusion barrier at the base of the cilium and prevents membrane-associated proteins from freely diffusing across it (Garcia et al. 2018). By removing the core TZ scaffolding component MKS-5, the structure of the TZ can be disrupted, presumably allowing proteins to enter the cilium more freely (Li et al. 2016; Jensen et al. 2015). Unexpectedly, this resulted in less entry of GCY-22 into the cilium, indicating that the TZ plays a role in import of GCY-22. In addition, we found that DAF-25, previously identified as essential for the proper localization of ciliary signaling proteins, is required for GCY-22 import into the cilium. Furthermore, we identified two domains within GCY-22 which, when deleted or mutated, affect entry of GCY-22 into the cilium: the dimerization domain and the RD3-binding domain.

Cilium tip localization

Once inside the cilium, GCY-22 is transported to the tip. Our results suggest that IFT is the primary driving force behind the sub-ciliary localization of GCY-22 at the cilium tip. Dual-color imaging of IFT and GCY-22::GFP showed that GCY-22::GFP co-localizes with the kinesin OSM-3 in a subset of the IFT particles, suggesting some accumulation of GCY-22::GFP in certain IFT particles or 'trains'. Most GCY-22::GFP tracks were significantly shorter than the IFT tracks, suggesting that cargo disembarks along the length of the cilium. Strikingly, many GCY-22::GFP particles moving in a retrograde

direction (towards the base) were picked up by IFT trains moving in the anterograde direction and relocalized to the tip. This behavior, not previously observed for other IFT-associated proteins, maintains a high density of receptor molecules at this compartment. How this is regulated—for example, whether this depends on differential affinity for the anterograde and the retrograde IFT machinery—remains to be determined. We also showed that when we interfere with IFT, either by using NaN_3 or disrupting the IFT components *bbs-8* or *osm-3*, accumulation of GCY-22::GFP at the tip is less efficient. These results indicate that IFT could be the main mechanism forming and maintaining the tip compartment. We cannot rule out that GCY-22 binds to other factors at the cilium tip, however, to date no such factors have been identified in *C. elegans* or other systems. For example, it remains unknown how components of Hedgehog signaling remain confined to the cilium tip (reviewed in (He et al. 2017)). Our data suggests that IFT could play an important role in such localizations by actively maintaining a specialized signaling compartment at the cilium tip.

To identify other proteins that play a role in the ciliary tip localization, we tested *daf-25*, *mks-5*, and *rdl-1* mutants. Only disrupting *mks-5* reduced the localization of GCY-22 at the cilium tip, which can be explained by the strongly reduced IFT mediated transport of GCY-22. Mutating *daf-25* completely abolished entry of GCY-22 into the cilium, making it unclear whether DAF-25 plays a role in tip localization. A *mks-5; daf-25* double mutant showed increased entry of GCY-22 compared to the *daf-25* single but still no tip localization, showing that the ciliary tip localization is *daf-25* dependent. However, it is also conceivable that other factors required for the formation of a cilium tip compartment are missing in these mutants.

Finally, none of the GCY-22::GFP protein domains tested in our deletion constructs were specifically required for cilium-tip localization. Such a function could however be masked by the lack of GCY-22::GFP in the cilium when the RD3 and dimerization domains of GCY-22 were deleted or mutated. Either of these domains could play a role in localization to the ciliary tip.

Ciliary proteins follow an intricate path from the ER and Golgi to their final destination in the cilium (Ranjan et al. 2019; Chadha et al. 2019). It is possible that DAF-25 is not directly involved in linking GCY-22 to the trafficking machinery, but instead is a more general component of the trafficking mechanism of ciliary proteins.

NaCl sensing by the cilium tip compartment

Whether GCY-22 is the NaCl receptor of the ASER neuron remains an open question. So far, genetic studies indicate that GCY-14 and GCY-22 confer specificity for NaCl in the ASE neurons (Ortiz et al. 2006; Ortiz et al. 2009; Smith et al. 2013). Notably, GCY-14 localizes similarly to GCY-22, i.e. to the base and tip of the cilium in the ASEL neuron (Murayama et al. 2013), and given their effect on chemotaxis to NaCl, GCY-14 and GCY-22 are likely the receptors of Na^+ and Cl^-, respectively. However, mutating GCY-22 affects chemotaxis to multiple compounds, although the strongest phenotype is in chemotaxis to NaCl (Ortiz et al. 2009). Others have suggested that a homodimer of GCY-22 is the receptor for Cl^- and that GCY-22 heterodimerizes with other GCYs in chemotaxis to other salts (Ortiz et al. 2009; Smith et al. 2013). Furthermore, GCY-14 and GCY-22 contain all the necessary amino acids to perform their function as homodimers (Murayama et al. 2013). We generated GCY-22::GFP(RD3-ala), GCY-22::spmCherry heterozygous animals to show the presence of GCY-22 homodimers. Because GCY-22::GFP(RD3-ala) proteins do not enter the cilium, a GFP signal in the cilium tip would only be possible if GCY-22:GFP(RD3-ala) dimerized with GCY-22::spmCh. We only detected mCherry in the cilium tip suggesting that GCY-22 does not form homodimers or, more likely, that the RD3 domain is needed for dimerization and secondarily cilium entry (data not shown).

The high concentration of GCY-22 at the ciliary tip suggests that the tip compartment is a highly sensitive detection apparatus, reminiscent of the high protein densities of rhodopsin in the mammalian photoreceptor cells and which are capable of detecting single photons (Baylor et al. 1979; Niu & Mitchell 2005). Mislocalization of GCY-22::RD3-ala::GFP affected chemotaxis to 1 mM NaCl most, suggesting that the ciliary tip compartment is required to navigate small differences in NaCl concentrations. It would be interesting to test this mutant on an assay with a shallow gradient instead of the steep gradient of our quadrant assay. In such an assay, the correct localization and high density of GCY-22 in the cilium tip could prove more important. On the other hand, the high packing density of rhodopsin limits lateral diffusion and slows the visual response (Calvert et al. 2001). Similar dynamics of high packing density could explain the relatively slow diffusion of GCY-22::GFP in the cilium tip, rather than binding to other cilium tip factors.

In the present study we investigated the role of a cGMP signaling compartment at the tip of a primary cilium. We showed the transporting route the receptor-type guanylate cyclase takes from cell body to the cilium tip, showed which protein domains are essential for correct localization of this receptor, and identify IFT as a key mechanism in establishing and maintaining this cilium tip compartment. Finally, we provide a first indication that the signaling compartment conveys high sensitivity to NaCl.

Methods

Strains and Constructs
Strains were cultured using standard methods (Brenner 1974). Alleles used in this research were: *kap-1(ok676)*, *osm-3(p802)*, *bbs-8(nx77), daf-25(m362), mks-5(tm3100).* The *Prab-3::mCherry::apt-9* construct was a gift from Angela Pasparaki and used for the cloning of *Pgpa-4::mCherry::tram-1.*

Microinjections
Microinjections were performed using standard methods (Mello & Fire 1995).

CRISPR/Cas9
To generate the *osm-3::mCherry* allele we injected animals with an injection mixture containing PU6::osm-3_sgRNA, Peft-3::cas9-SV40_NLS::tbb-2, *rol-6*, and a plasmid containing the mCherry template with 1500 bp homology arms. Animals were injected and placed on separate plates. Three days later, F1 offspring was picked, allowed to self-reproduce, and screened by PCR.

We used the *dpy-10* based the co-CRISPR method (Ward, 2015) and a PCR template of GFP with 35 bp homology arms to generate the *gcy-22::GFP* allele, and a ssODN template with 35 bp homology arms to generate the *gcy-22(RD3<Ala)::GFP* and *gcy-22::spmCherry* alleles. We generated the *rdl-1(gj1989)* allele using two sgRNAs and no template.

Microscopy
Animals were immobilized on a 6% agarose pad, 0.10 µm polystyrene microspheres (Polybead, Polysciences Inc.), and 10 mM Levamisole (Sigma) in M9 buffer as an anesthetic, unless stated otherwise.
Fluorescence images were taken using an inverted spinning disc confocal microscope (Nikon Ti-eclipse) with an EM CCD camera (QuantEM512C, Photometrics) and Metamorph Imaging software, unless stated otherwise. Images were analyzed using FIJI software (version 2.0.0). For FRAP experiments, a FRAP3D unit (ROPER) was used. For the time-lapse images, animals were immobilized on a 6% agarose pad and M9 containing 10 mM Levamisole. Images were taken at 300ms intervals and Peterman plugins KymographClear 1.0. Kymograms were analyzed using a custom FIJI plugin written by I. Smal. Dual color time-lapse images were taken using a DV2

beamsplitter (MAG Biosystems). Quantification of GCY-22::GFP fluorescence in different mutant backgrounds, and of GFP molecules at the cilium tip, was performed on a laser scanning confocal microscope (SP5 AOBS, Leica). A purified GFP sample (gift from G. Kremer) was used to generate a calibration curve for the quantification of GFP.

NaN_3

To stop ATP production, Sodium Azide (Sigma) was added to a 6% agarose pads at a concentration of 20 mM. Imaging started 10 min after immobilization. Animals were incubated in a drop of M9 containing 20 mM NaN_3 before proceding with standard immobilisation with microspheres and Levamisol.

Chemotaxis assays

The quadrant assay used to asses chemotaxis to NaCl was adapted from Wicks *et al.* and Jansen *et al.* (Wicks et al. 2000; Jansen et al. 2002). Briefly, two diagonally opposite quadrants of a sectional petri dish (Star Dish, Phoenix Biomedical) were filled with 13.5 mL buffered agar (1.7% Agar, 5 mM K_2HPO_4, 5 mM KH_2PO_4, 1 mM $CaCl_2$ and 1 mM $MgSO_4$) containing NaCl and two diagonally opposite quadrants with 13.5 mL buffered agar without NaCl. Immediately before the assay, the plastic dividers between the quadrants were covered with a thin layer of agar. Age synchronized *C. elegans* populations were washed 3 times for 5 min with CTX buffer (5 mM K_2HPO_4, 5 mM KH_2PO_4, 1 mM $CaCl_2$ and 1 mM $MgSO_4$). Approximately 100 animals were placed in the middle of a sectional dish. After 10 min, animals on each quadrant were counted and a chemotaxis index (CI) was calculated for each plate (CI = (# animals on NaCl – # animals not no NaCl)/ total # animals). To determine the CI of a strain, 2 assays per day were performed for at least 3 days.

Statistics

Statistical analyses were performed using R software, version 3.6.0. For the chemotaxis assays a one-way ANOVA was performed, followed by a pairwise-t-test with Holm correction for multiple comparisons. FRAP curves were fitted using R software.

Acknowledgements

We are grateful to the Erasmus MC Optical Imaging Centre for their support. We thank C.L. van der Burght for insightful discussions on statistical analyses. Some strains were provided by the CGC, which is funded by NIH Office of Research Infrastructure Programs (P40 OD010440), and the NBRP. This work is part of the research program of the Foundation for Fundamental Research on Matter (FOM), which is financially supported by the Netherlands Organization for Scientific Research (NWO).

Author Contributions

S.N.B., M.R.L. and G.J. conceived the study. S.N.B. and S.R. generated strains, performed experiments and analyzed the data. J.J. and C.L. generated strains, performed experiments and analyzed the data for the construct-based domain deletion experiments. S.N.B., G.J., and M.R.L. wrote the manuscript.

References

Azadi, Seifollah; Molday, Laurie L & Molday, Robert S. 2010. «RD3, the protein associated with Leber congenital amaurosis type 12, is required for guanylate cyclase trafficking in photoreceptor cells». *Proceedings of the National Academy of Sciences* 107 (49): 21158–21163. doi:10.1073/pnas.1010460107 .

Baylor, DA; Lamb, TD & Yau, KW. 1979. «Responses of retinal rods to single photons.» *The Journal of Physiology* 288 (1): 613–634. doi:10.1113/jphysiol.1979.sp012716 .

Birnby, DA et al. 2000. «A transmembrane guanylyl cyclase (DAF-11) and Hsp90 (DAF-21) regulate a common set of chemosensory behaviors in caenorhabditis elegans.» *Genetics* 155 (1): 85 104. doi:10.1006/jmbi.1990.9999 .

Brear, Andrea G et al. 2014. «Diverse Cell Type-Specific Mechanisms Localize G Protein-Coupled Receptors to Caenorhabditis elegans Sensory Cilia». *Genetics* 197 (2): 667–684. doi:10.1534/genetics.114.161349 .

Calvert, PD et al. 2001. «Membrane protein diffusion sets the speed of rod phototransduction». *Nature* 411 (6833): 90. doi:10.1038/35075083 .

Chadha, Abhishek et al. 2019. «The route of the visual receptor, rhodopsin, along the cilium». *J Cell Sci*: jcs.229526. doi:10.1242/jcs.229526 .

Endoh-Yamagami, Setsu et al. 2009. «The Mammalian Cos2 Homolog Kif7 Plays an Essential Role in Modulating Hh Signal Transduction during Development». *Current Biology* 19 (15): 1320–1326. doi:10.1016/j.cub.2009.06.046 .

Etchberger, John F et al. 2007. «The molecular signature and cis-regulatory architecture of a C. elegans gustatory neuron». *Genes & Development* 21 (13): 1653–1674. doi:10.1101/gad.1560107 .

Fotiadis, Dimitrios et al. 2003. «Atomic-force microscopy: Rhodopsin dimers in native disc membranes». *Nature* 421 (6919): 421127a. doi:10.1038/421127a .

Fujiwara, Manabi et al. 2010. «A Novel zf-MYND Protein, CHB-3, Mediates Guanylyl Cyclase Localization to Sensory Cilia and Controls Body Size of Caenorhabditis elegans». *PLoS Genetics* 6 (11): e1001211. doi:10.1371/journal.pgen.1001211 .

Garcia, Galo; Raleigh, David R & Reiter, Jeremy F. 2018. «How the Ciliary Membrane Is Organized Inside-Out to Communicate Outside-In.» *Current biology : CB* 28 (8): R421–R434. doi:10.1016/j.cub.2018.03.010 .

Hao, Limin et al. 2011. «Intraflagellar transport delivers tubulin isotypes to sensory cilium middle and distal segments». *Nature Cell Biology* 13 (7): 790. doi:10.1038/ncb2268 .

He, Mu et al. 2014. «The kinesin-4 protein Kif7 regulates mammalian Hedgehog signalling by organizing the cilium tip compartment». *Nature cell biology* 16 (7): 663 672. doi:10.1038/ncb2988 .

He, Mu; Agbu, Stephanie & Anderson, Kathryn V. 2017. «Microtubule Motors Drive Hedgehog Signaling in Primary Cilia». *Trends in Cell Biology* 27 (2): 110–125. doi:10.1016/j.tcb.2016.09.010 .

Jensen, Victor L et al. 2010. «Localization of a Guanylyl Cyclase to Chemosensory Cilia Requires the Novel Ciliary MYND Domain Protein DAF-25». *PLoS Genetics* 6 (11): e1001199. doi:10.1371/journal.pgen.1001199 .

———. 2015. «Formation of the transition zone by Mks5/Rpgrip1L establishes a ciliary zone of

exclusion (CIZE) that compartmentalises ciliary signalling proteins and controls PIP2 ciliary abundance». *The EMBO Journal* 34 (20): 2537–2556. doi:10.15252/embj.201488044 .

Kim, Kyuhyung et al. 2009. «Two Chemoreceptors Mediate Developmental Effects of Dauer Pheromone in C. elegans». *Science* 326 (5955): 994–998. doi:10.1126/science.1176331 .

Klink, Björn et al. 2017. «A recombinant BBSome core complex and how it interacts with ciliary cargo». *eLife* 6: e27434. doi:10.7554/elife.27434 .

Lechtreck, Karl F. 2015. «IFT–Cargo Interactions and Protein Transport in Cilia». *Trends in Biochemical Sciences* 40 (12): 765–778. doi:10.1016/j.tibs.2015.09.003 .

Li, Chunmei et al. 2016. «MKS5 and CEP290 Dependent Assembly Pathway of the Ciliary Transition Zone». *PLOS Biology* 14 (3): e1002416. doi:10.1371/journal.pbio.1002416 .

Liem, Karel F et al. 2009. «Mouse Kif7/Costal2 is a cilia-associated protein that regulates Sonic hedgehog signaling». *Proceedings of the National Academy of Sciences* 106 (32): 13377–13382. doi:10.1073/pnas.0906944106 .

Lienkamp, Soeren; Ganner, Athina & Walz, Gerd. 2012. «Inversin, Wnt signaling and primary cilia». *Differentiation* 83 (2): S49–S55. doi:10.1016/j.diff.2011.11.012 .

Liu, Peiwei & Lechtreck, Karl F. 2018. «The Bardet–Biedl syndrome protein complex is an adapter expanding the cargo range of intraflagellar transport trains for ciliary export». *PNAS* 121 (5): 201713226 E943. doi:10.1073/pnas.1713226115 .

Ludington, William B et al. 2013. «Avalanche-like behavior in ciliary import». *Proceedings of the National Academy of Sciences* 110 (10): 3925–3930. doi:10.1073/pnas.1217354110 .

Martínez-Velázquez, Luis A & Ringstad, Niels. 2018. «Antagonistic regulation of trafficking to Caenorhabditis elegans sensory cilia by a Retinal Degeneration 3 homolog and retromer». *Proceedings of the National Academy of Sciences* 115 (3): E438 E447. doi:10.1073/pnas.1712302115 .

McGrath, Patrick T et al. 2011. «Parallel evolution of domesticated Caenorhabditis species targets pheromone receptor genes». *Nature* 477 (7364): 321. doi:10.1038/nature10378 .

Mello, Craig & Fire, Andrew. 1995. «Methods in Cell Biology». *Methods in Cell Biology* 48: 451–482. doi:10.1016/s0091-679x(08)61399-0 .

Mondal, Sudip et al. 2011. «Imaging in vivo Neuronal Transport in Genetic Model Organisms Using Microfluidic Devices». *Traffic* 12 (4): 372–385. doi:10.1111/j.1600-0854.2010.01157.x .

Murayama, Takashi et al. 2013. «Environmental Alkalinity Sensing Mediated by the Transmembrane Guanylyl Cyclase GCY-14 in C. elegans». *Current Biology* 23 (11): 1007–1012. doi:10.1016/j.cub.2013.04.052 .

Nakayama, Kazuhisa & Katoh, Yohei. 2018. «Ciliary protein trafficking mediated by IFT and BBSome complexes with the aid of kinesin-2 and dynein-2 motors.» *Journal of biochemistry* 163 (3): 155–164. doi:10.1093/jb/mvx087 .

Nishimura, Darryl Y et al. 2004. «Bbs2-null mice have neurosensory deficits, a defect in social dominance, and retinopathy associated with mislocalization of rhodopsin». *Proceedings of the National Academy of Sciences of the United States of America* 101 (47): 16588–16593. doi:10.1073/pnas.0405496101 .

Niu, Shui-Lin & Mitchell, Drake C. 2005. «Effect of Packing Density on Rhodopsin Stability and Function in Polyunsaturated Membranes». *Biophysical Journal* 89 (3): 1833–1840. doi:10.1529/biophysj.105.061812 .

Ortiz, Christopher O et al. 2006. «Searching for neuronal left/right asymmetry: genomewide analysis of nematode receptor-type guanylyl cyclases.» *Genetics* 173 (1): 131 149. doi:10.1534/genetics.106.055749 .

———. 2009. «Lateralized gustatory behavior of C. elegans is controlled by specific receptor-type guanylyl cyclases.» *Current Biology* 19 (12): 996 1004. doi:10.1016/j.cub.2009.05.043 .

Oswald, Felix et al. 2018. «Interplay between Ciliary Ultrastructure and IFT-Train Dynamics Revealed by Single-Molecule Super-resolution Imaging». *Cell reports* 25 (1): 224 235. doi:10.1016/j.celrep.2018.09.019 .

Prevo, Bram et al. 2015. «Functional differentiation of cooperating kinesin-2 motors orchestrates cargo import and transport in C. elegans cilia». *Nature Cell Biology* 17 (12): 1536–1545. doi:10.1038/ncb3263 .

Qin, Hongmin et al. 2005. «Intraflagellar Transport Is Required for the Vectorial Movement of TRPV Channels in the Ciliary Membrane». *Current Biology* 15 (18): 1695–1699. doi:10.1016/j.cub.2005.08.047 .

Ranjan, Peeyush; Awasthi, Mayanka & Snell, William J. 2019. «Transient Internalization and Microtubule-Dependent Trafficking of a Ciliary Signaling Receptor from the Plasma Membrane to the Cilium». *Current Biology*. doi:10.1016/j.cub.2019.07.022 .

Reiter, Jeremy F & Leroux, Michel R. 2017. «Genes and molecular pathways underpinning ciliopathies». *Nature Reviews Molecular Cell Biology* 18 (9): 533. doi:10.1038/nrm.2017.60 .

Rieke, F & Baylor, DA. 1998. «Single-photon detection by rod cells of the retina». *Reviews of Modern Physics* 70 (3): 1027–1036. doi:10.1103/revmodphys.70.1027 .

Smith, Heidi K et al. 2013. «Defining Specificity Determinants of cGMP Mediated Gustatory Sensory Transduction in Caenorhabditis elegans». *Genetics* 194 (4): 885–901. doi:10.1534/genetics.113.152660 .

Wicks, Stephen R et al. 2000. «CHE-3, a Cytosolic Dynein Heavy Chain, Is Required for Sensory Cilia Structure and Function in Caenorhabditis elegans». *Developmental Biology* 221 (2): 295–307. doi:10.1006/dbio.2000.9686 .

Williams, Corey L et al. 2011. «MKS and NPHP modules cooperate to establish basal body/transition zone membrane associations and ciliary gate function during ciliogenesis». *The Journal of Cell Biology* 192 (6): 1023–1041. doi:10.1083/jcb.201012116 .

Wojtyniak, Martin et al. 2013. «Cell- and subunit-specific mechanisms of CNG channel ciliary trafficking and localization in C. elegans.» *Journal of cell science* 126 (Pt 19): 4381 4395. doi:10.1242/jcs.127274 .

Ye, Fan et al. 2013. «Single molecule imaging reveals a major role for diffusion in the exploration of ciliary space by signaling receptors». *eLife* 2: e00654. doi:10.7554/elife.00654 .

Ye, Fan; Nager, Andrew R & Nachury, Maxence V. 2018. «BBSome trains remove activated GPCRs from cilia by enabling passage through the transition zone». *J Cell Biol* 217 (5): jcb.201709041. doi:10.1083/jcb.201709041 .

Zhang, Houbin et al. 2014. «Mistrafficking of prenylated proteins causes retinitis pigmentosa 2». *The FASEB Journal* 29 (3): 932–942. doi:10.1096/fj.14-257915 .

Zulliger, Rahel et al. 2015. «Impaired Association of Retinal Degeneration-3 with Guanylate Cyclase-1 and Guanylate Cyclase-activating Protein-1 Leads to Leber Congenital Amaurosis-1». *Journal of Biological Chemistry* 290 (6): 3488–3499. doi:10.1074/jbc.m114.616656 .

Figure 1. GCY-22::GFP localizes to the cell-body, is transported along the dendrite and localizes to the PCMC and cilium tip in the ASER neuron.
(A) Schematic of the head of the animal showing the ASER cellbody, dendrite and cilium. Inserts: Fluorescence images with GCY-22::GFP (green) and *flp-6p::mCherry* (red) showing localization in the cell body, vesicle in the dendrite and localization to the PCMC and tip of the cilium. (B) Ectopic expression of GCY-22::GFP in the ASI neuron showing localization at the PCMC and cilium tip. (C) Quantification of GCY-22::GFP molecules at the cilium tip of the ASER neuron.

Figure 2. GCY-22::GFP localizes to stable pools at the PCMC and cilium tip. (A) Fluorescence recovery after photobleaching the entire cilium tip compartment. (B) Fluorescence recovery after photobleaching the entire PCMC. (C) Fluorescence recovery after photobleaching half of the tip compartment. (D) Fluorescence recovery after photobleaching half of the PCMC.

Figure 3. The cilium tip compartment is actively maintained by IFT. (A) Kymogram of GCY-22::GFP showing anterograde and retrograde transport and diffusion tracks. (B) Kymograms showing overlap of IFT tracks of GCY-22::GFP (green) and OSM-3::mCherry (red). (C) Quantification of GCY-22::GFP (green), OSM-3::mCherry (left graph, red), and XBX::tdTomato (right graph, red) tracks. (D) Fluorescence images showing localization of GCY-22::GFP in PCMC and cilium in different mutant backgrounds. (E) Quantification of normalized fluorescence intensity in different mutant backgrounds of GCY-22::GFP in the PCMC, axoneme and cilium tip.

Figure 4. Maintenance of cilium tip compartment is ATP dependent. (A) Fluorescence images of GCY-22::GFP showing cilium tip collapse and kymograms of OSM-3:mCherry showing IFT arrest after NaN_3 treatment. (B) Quantification of cilium tip and cilium length, and distal segment IFT after NaN_3 treatment. (C) Fluorescence images showing recovery of the cilium tip compartment after 30 min of NaN_3 treatment.

Figure 5. Cilium tip localization of GCY-22::GFP requires the dimerization and RD3-associated domains. Schematic of different versions of *gcy-22::GFP* deletion constructs showing deleted or replaced domains. Fluorescence images showing localization of corresponding GCY-22::GFP deletion constructs (green), and *Pgcy-7::xbx-1::tdTomato*.

Figure 6. Cilium tip localization of GCY-22 is required for sensitive detection of NaCl. (A) Chemotaxis of different mutants shows wild type response of *gcy-22::GFP* animals and involvement of GCY-22 and GCY-14. (B) Chemotaxis to 1 mM, 10 mM and 100 mM requires OSM-3, and BBS-8 for chemotaxis to 1 mM and 100 mM. (C) Chemotaxis to 1 mM, 10 mM, and 100 mM NaCl requires DAF-25, and MKS-5 to 1 mM and 10 mM. (D) Chemotaxis to 1 and 10 mM requires cilium tip localization of GCY-22.

Figure 1

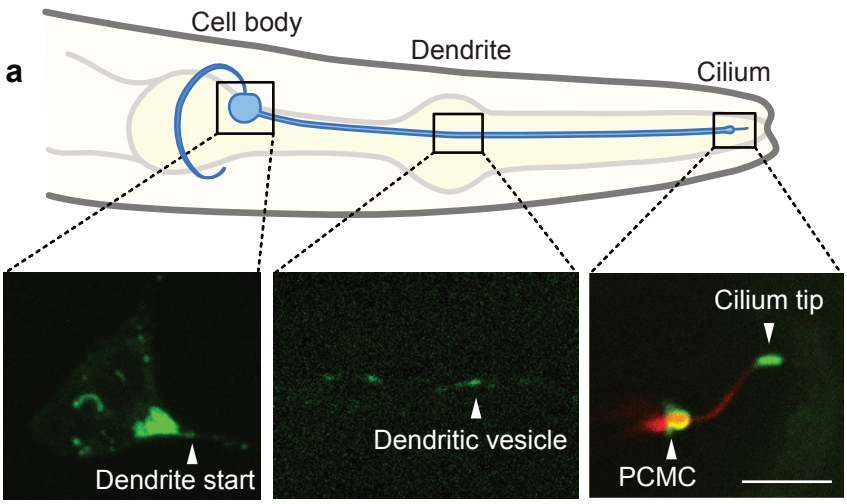
a
Cell body
Dendrite
Cilium
Dendrite start
Dendritic vesicle
Cilium tip
PCMC

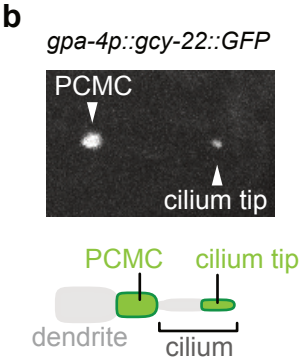
b
gpa-4p::gcy-22::GFP
PCMC
cilium tip
PCMC
cilium tip
dendrite
cilium

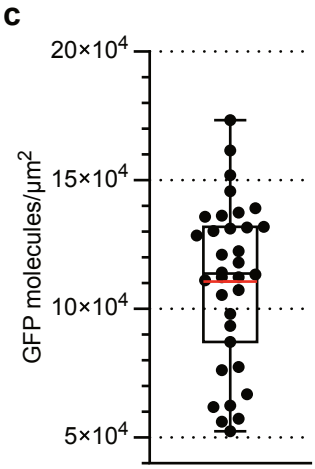
c
20×10^4
15×10^4
10×10^4
5×10^4
GFP molecules/μm^2

Figure 2

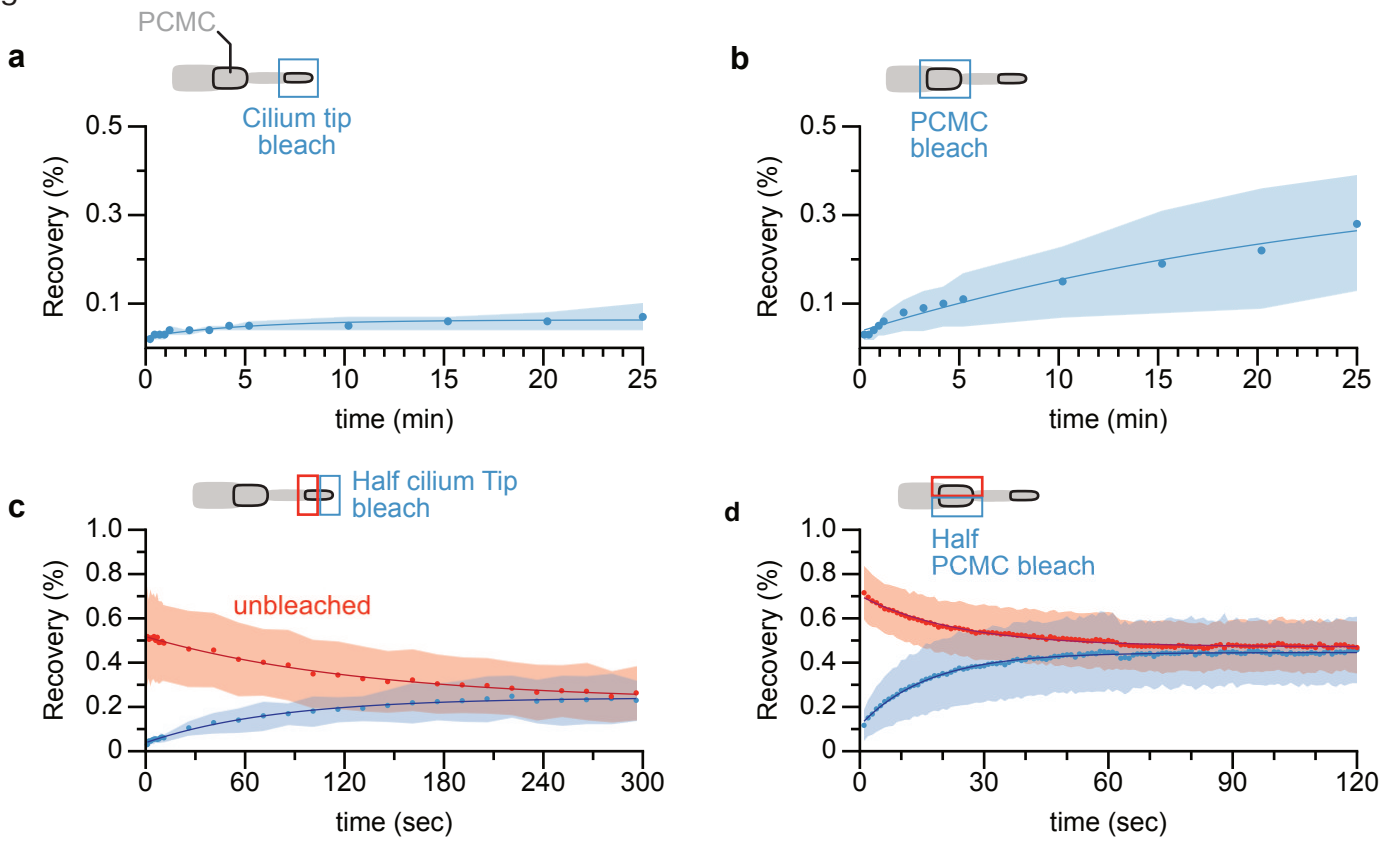
a
PCMC
Cilium tip
bleach
Recovery (%)
0.5
0.3
0.1
0
5
10
15
20
25
time (min)
b
PCMC
bleach
Recovery (%)
0.5
0.3
0.1
0
5
10
15
20
25
time (min)
c
Half cilium Tip
bleach
unbleached
Recovery (%)
1.0
0.8
0.6
0.4
0.2
0
60
120
180
240
300
time (sec)
d
Half
PCMC bleach
Recovery (%)
1.0
0.8
0.6
0.4
0.2
0
30
60
90
120
time (sec)

Figure 3

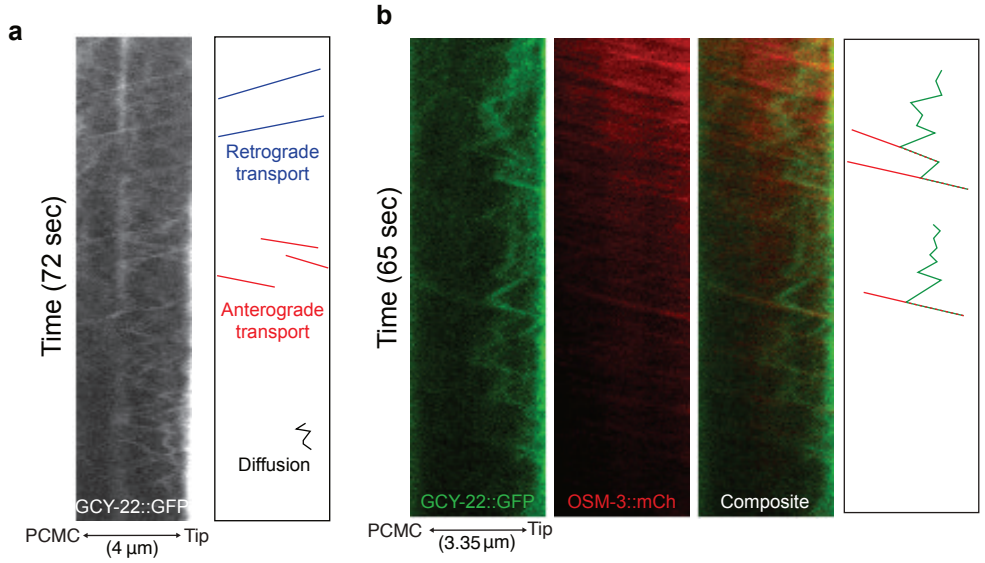
a
Time (72 sec)
GCY-22::GFP
PCMC
Tip
(4 µm)
Retrograde transport
Anterograde transport
Diffusion
b
Time (65 sec)
GCY-22::GFP
OSM-3::mCh
Composite
PCMC
Tip
(3.35 µm)

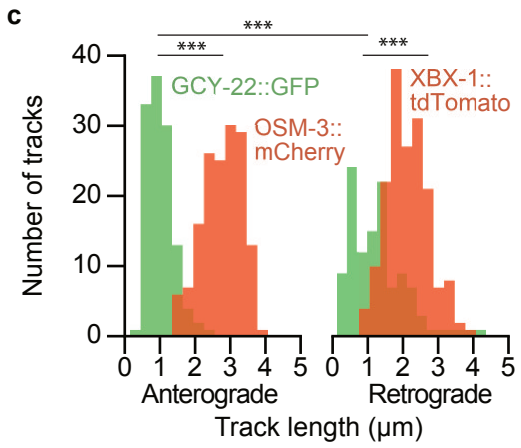
c
Number of tracks
GCY-22::GFP
OSM-3::mCherry
XBX-1::tdTomato
***
***
***
Anterograde
Retrograde
Track length (µm)

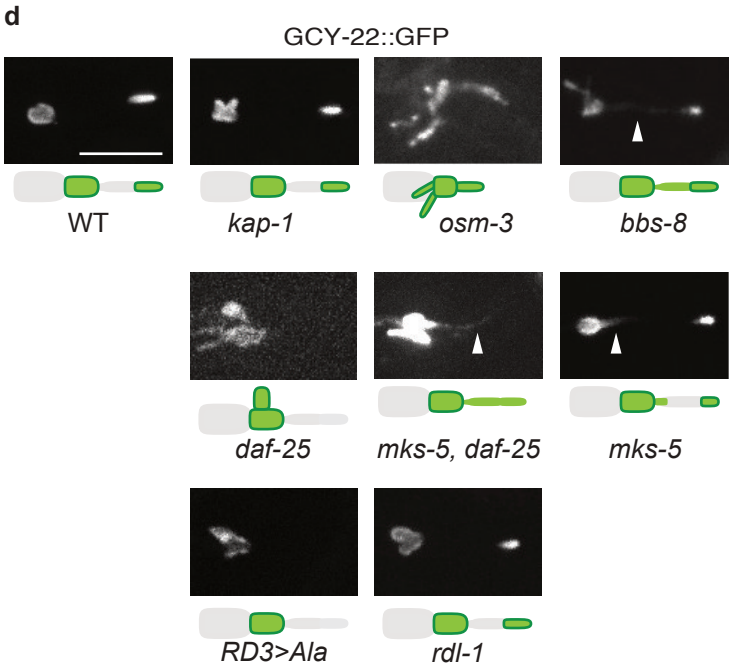
d
GCY-22::GFP
WT
kap-1
osm-3
bbs-8
daf-25
mks-5, daf-25
mks-5
RD3>Ala
rdl-1

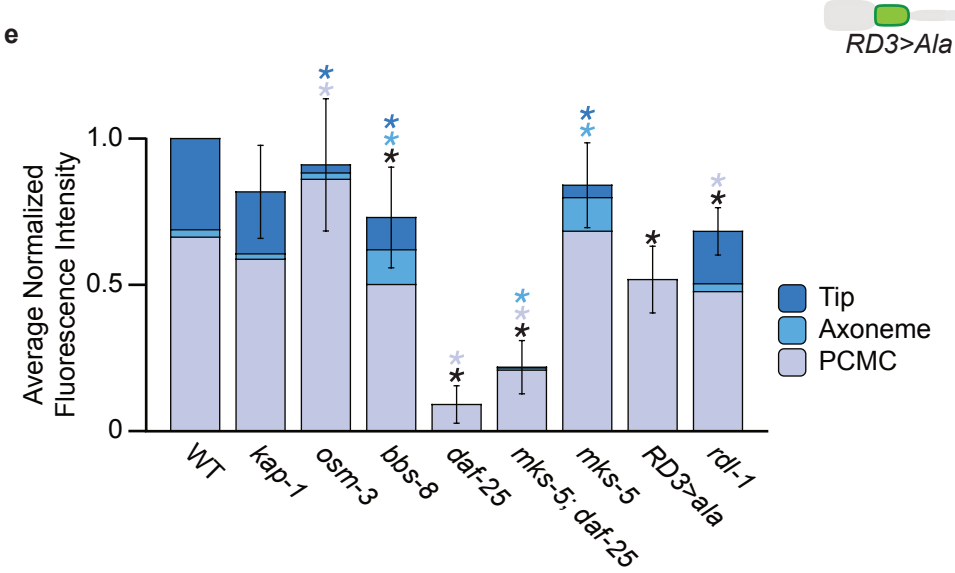
e
Average Normalized Fluorescence Intensity
Tip
Axoneme
PCMC
WT
kap-1
osm-3
bbs-8
daf-25
mks-5; daf-25
mks-5
RD3>ala
rdl-1

Figure 4

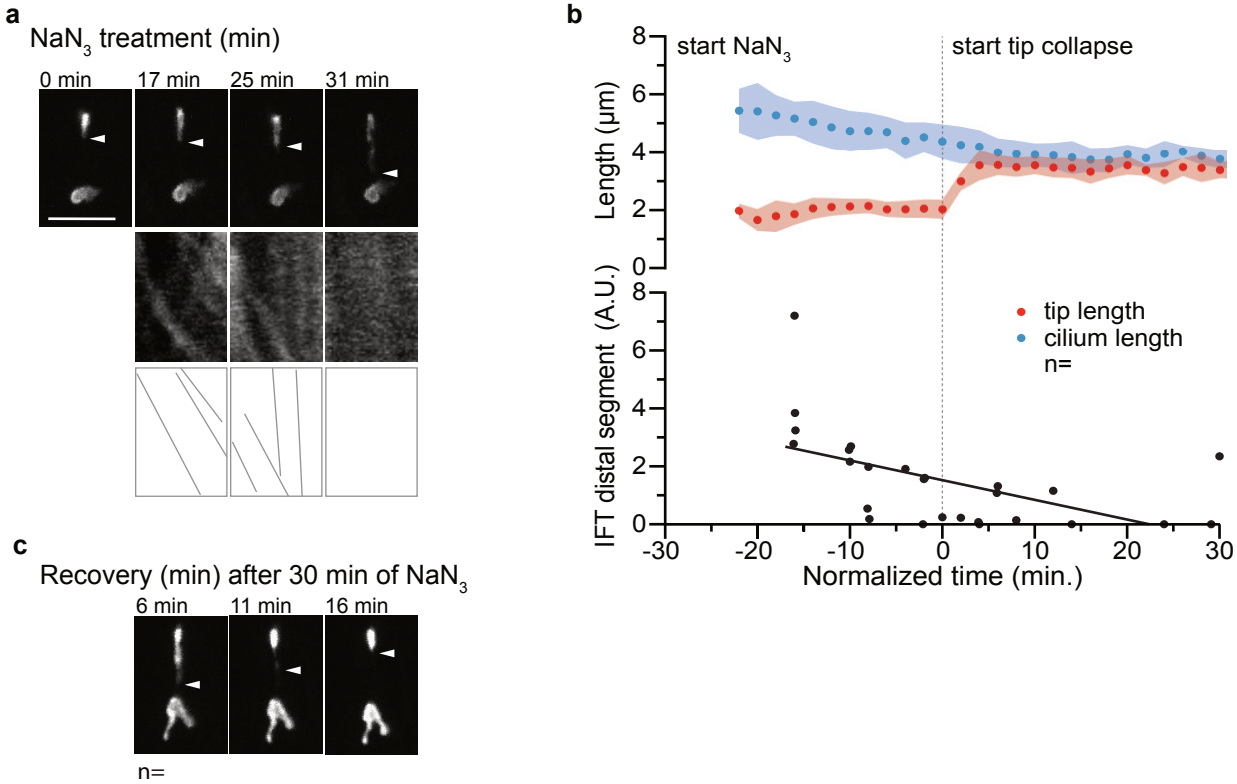
a
NaN3 treatment (min)
0 min
17 min
25 min
31 min
b
start NaN3
start tip collapse
Length (µm)
IFT distal segment (A.U.)
tip length
cilium length
n=
Normalized time (min.)
c
Recovery (min) after 30 min of NaN3
6 min
11 min
16 min
n=

Figure 5

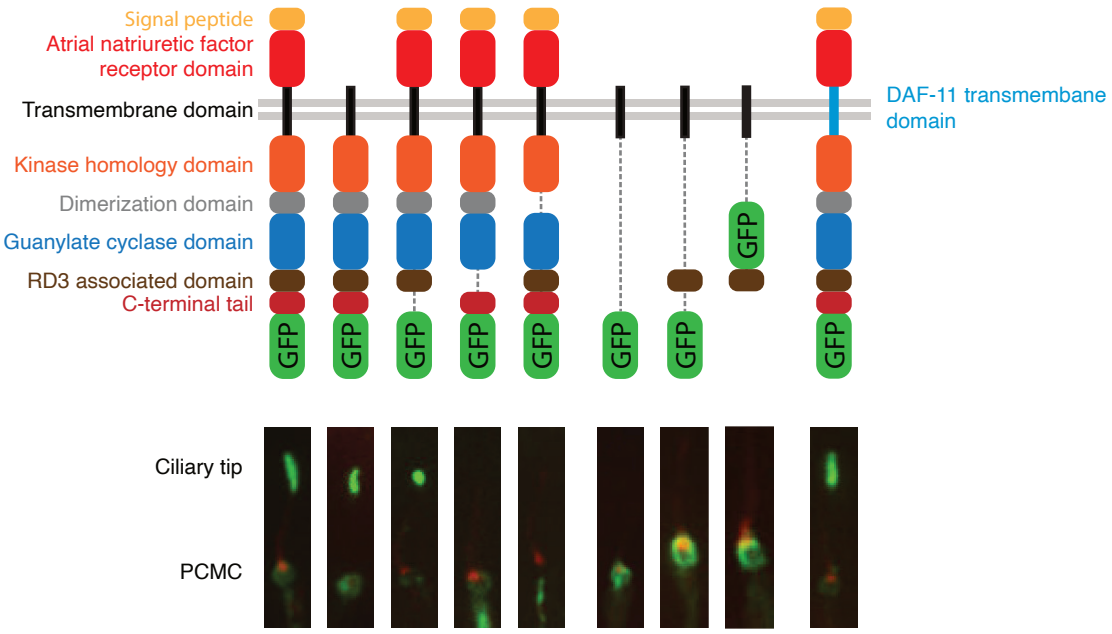

GCY-22 construct::GFP, XBX-1::tdTomato

Figure 6.

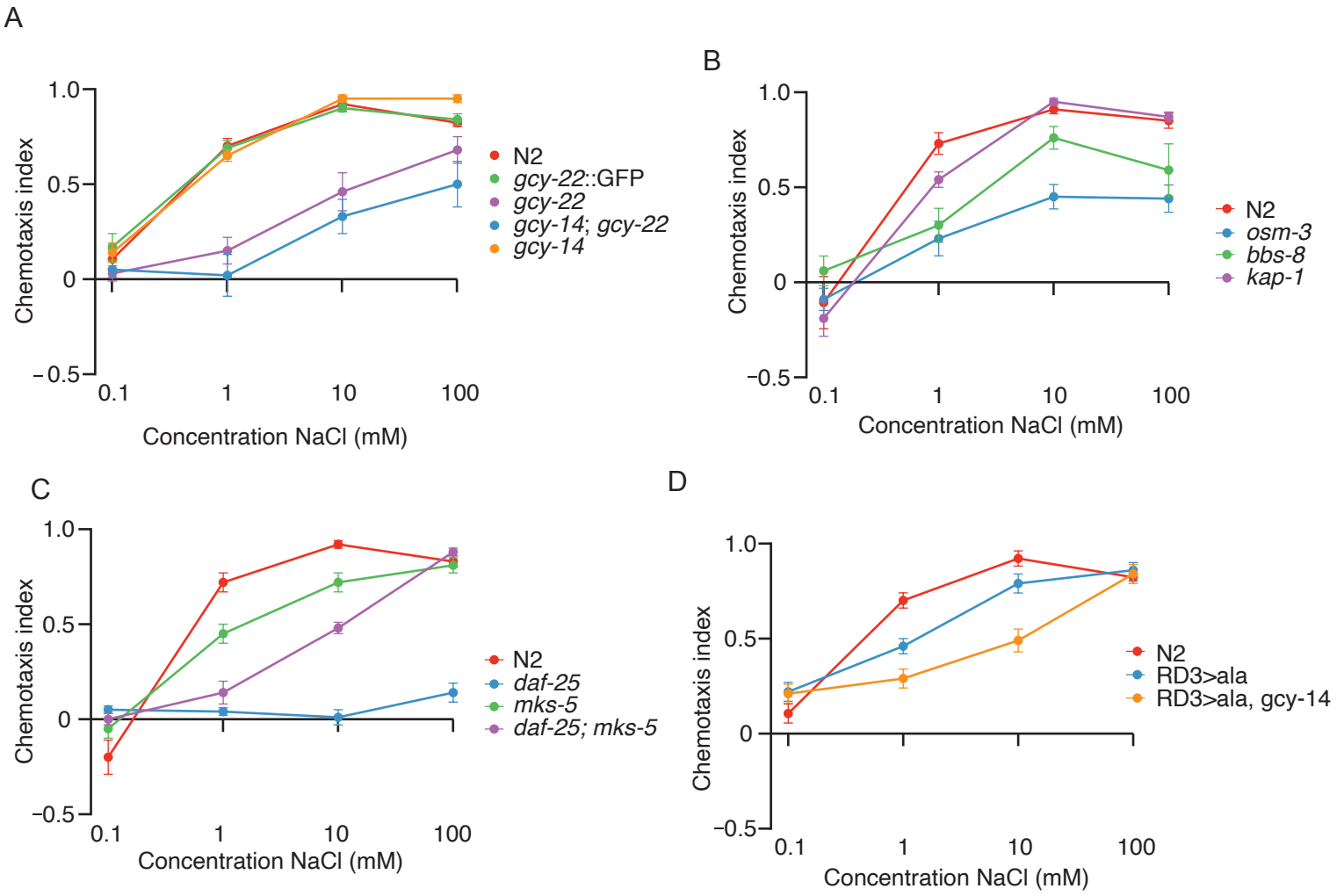
A
Chemotaxis index
1.0
0.5
0
−0.5
0.1
1
10
100
Concentration NaCl (mM)
N2
gcy-22::GFP
gcy-22
gcy-14; gcy-22
gcy-14
B
Chemotaxis index
1.0
0.5
0
−0.5
0.1
1
10
100
Concentration NaCl (mM)
N2
osm-3
bbs-8
kap-1
C
Chemotaxis index
1.0
0.5
0
−0.5
0.1
1
10
100
Concentration NaCl (mM)
N2
daf-25
mks-5
daf-25; mks-5
D
Chemotaxis index
1.0
0.5
0
−0.5
0.1
1
10
100
Concentration NaCl (mM)
N2
RD3>ala
RD3>ala, gcy-14

Table 1. GCY-22::GFP IFT tracks in different mutant backgrounds.

Genotype	# animals with tracks (total # animals)	Significance	Average IFT tracks /min anterograde	Significance	retrograde	Significance
WT	17(18)	-	6.14(±3.61)	-	6.71(±3.71)	-
kap-1	16(18)	-	9.47(±6.70)	-	6.53(±4.71)	-
osm-3	7(13)	**	1.75(±1.92)	*	0.88(±1.16)	***
bbs-8	12(17)	-	2.58(±3.22)	-	0.92(±1.12)	***
daf-25	0(18)	***	-	-	-	-
mks-5; daf-25	4(21)	***	0.89(±1.99)	***	0.23(±0.58)	***
mks-5	5(14)	***	1.67(±2.77)	*	0.43(±1.01)	***
gcy-22(RD3-Ala)	0(16)	***	-	-	-	-
rdl-1	9(13)	-	2.63(±2.72)	-	3.14(±3.86)	*